Arabian Journal of Chemistry (2023) **16**, 104884

King Saud University

Arabian Journal of Chemistry

www.ksu.edu.sa
www.sciencedirect.com

ORIGINAL ARTICLE

In vitro/*vivo* antifungal activity study of novel mandelic acid derivatives as potential fungicides against *Thanatephorus cucumeris*

Huabin Shi, Longju Li, Dandan Song, Ya Zheng, Zhibing Wu *

National Key Laboratory of Green Pesticide, Key Laboratory of Green Pesticide and Agricultural Bioengineering, Ministry of Education, Center for R&D of Fine Chemicals of Guizhou University, Guiyang 550025, China

Received 15 February 2023; accepted 2 April 2023
Available online 11 April 2023

KEYWORDS

Mandelic acid;
1,3,4-thiadiazole thioether;
Antifungal activity;
Sclerotia formation, sclerotia germination;
Antifungal mechanism study

Abstract To discover highly efficient and novel lead compounds against *Thanatephorus cucumeris*, a series of novel mandelic acid derivatives containing 1,3,4-thiadiazole thioether was designed and synthesized. The bioassay results revealed that target compound $\mathbf{F_{10}}$ exhibited excellent antifungal activity against *T. cucumeris* with EC_{50} value of 9.7 μg/mL. Further studies found that $\mathbf{F_{10}}$ not only significantly inhibited the growth of *T. cucumeris* mycelia but also effectively inhibited the formation of sclerotia, and exhibited significant *in vivo* protective (61.1%) and curative (67.9%) activities at 200 μg/mL. Mechanism studies demonstrated that $\mathbf{F_{10}}$ can damage the integrity of the cell membrane structure, resulting in increased permeability of the cell membrane, releasing the intracellular electrolyte and inhibiting the growth of fungi. In general, this work is helpful for managing the formation and diffusion of the infection source and provides an effective method to control rice sheath blight disease infected with sclerotia of *T. cucumeris*.

1. Introduction

Plant diseases are an important factor that can affect agricultural production (Ghorbanpour et al., 2018; Giray et al., 2020); in particular, plant diseases caused by fungi are one of the most serious threats to global crop production, food quality, and security (Chen et al., 2019b; Li et al., 2019a; Ma et al., 2019; Yang et al., 2019a; Yin et al., 2020; Dong et al., 2022). According to statistics, approximately 10% to 16% of the crop yield reduction in the world is caused by pathogenic fungi each year, and the average economic losses exceeded $220 billion (Fisher et al., 2012; Li, et al., 2019b; Yan et al., 2020; Tudi et al., 2021; Sun et al., 2022). Among the pathogenic fungi, *Thanatephorus cucumeris* (anamorph: *Rhizoctonia solani*) causes rice sheath blight, which is one of the most extensive and destructive fungal diseases in many rice-growing areas (Feng et al., 2017; Persaud et al., 2019). Its dispersal and propagation are mediated by sclerotia, aggregations of hyphae, and it can germinate a mass of hyphae under various environments (Basu et al., 2016; Lu et al., 2016; Tiwari et al., 2017). The infection process of plants with *T. cucumeris* is shown in Figure S1. Long-term persistence of the sclerotia and hyphae in the agricultural landscape is achieved by quiescent survival on plant deb-

* Corresponding author.
E-mail addresses: zbwu@gzu.edu.cn, wzb1171@163.com (Z. Wu).

Peer review under responsibility of King Saud University.

Production and hosting by Elsevier

https://doi.org/10.1016/j.arabjc.2023.104884

ris, and *T. cucumeris* overwinter on straw stubble before infecting a secondary host, leading to the outbreak of disease (Fisher et al., 2012; Suwannarach et al., 2012). Sclerotia and hyphae play crucial roles in the life and infection cycle. Although many attempts have been made to treat rice sheath blight using new technology, the control of *T. cucumeris* still mainly relies on the utilization of chemical fungicides (Ashkani et al., 2015; Ke et al., 2017; Roese et al., 2018). It would be hugely attractive to develop a fungicide with strong inhibitory action on mycelial development, sclerotia formation or germination of *T. cucumeris* in one study.

1,3,4-thiadiazole is a well-known important heterocyclic compound, and its derivatives have broad-spectrum biological activities, such as antimicrobial (Mao et al., 2021), insecticidal (Chen et al., 2019a), antiviral (Gan et al., 2017), and antitumor activities (Chen et al., 2019c). Mandelic acid, as a prodrug, has been used to treat urinary infections and develop antithrombotic, antibiotic, and antitumor drugs since the early 20th century (El and Gould 2016; Saeed et al., 2017; Li et al., 2021). Mandipropamid, the only commercial mandelic acid fungicide in the field of pesticides, was put on the market in 2001. There are few reports on the antifungal activity of mandelic acid derivatives in the agricultural field, which provides an opportunity for molecular derivation.

To obtain the lead compounds as potential antifungal agents, a series of novel mandelic acid derivatives containing 1,3,4-thiadiazole thioether were designed and synthesized (Fig. 1). Bioassay evaluation found that the target compounds exhibited excellent *in vitro*/*vivo* antifungal activities against *T. cucumeris*, and the effect on the formation and germination of *T. cucumeris* sclerotia after treatment with highly active compounds was further explored. Then, the *in vitro* antifungal mechanism against *T. cucumeris* was studied.

2. Materials and methods

2.1. Instruments and chemicals

^{1}H, ^{13}C, and ^{19}F NMR spectra were obtained by a Bruker 400 NMR spectrometer (Bruker Corporation, Germany) or JEOL-ECX 500 NMR (JEOL Corporation, Japan) using TMS as an internal standard and $CDCl_3$ or DMSO d_6 as the solvent. HRMS data were obtained on a Thermo Scientific Q Exactive mass spectrometer (Thermo Scientific, USA). X-ray crystallographic data were collected by a Bruker Corporation diffractometer (Bruker Corporation, Germany). Melting points were measured on an XT-4 binocular microscope melting point apparatus and were uncorrected. The morphology of mycelia was observed by a Nova Nano SEM450 scanning electron microscope (Thermo Fisher Scientific, USA) and an Olympus-BX53F fluorescence microscope (Olympus-BX53F, Olympus, Japan). Electrical conductivity was measured using a DDS-307 conductivity meter (INESA & Scientific Instrument Co., Ltd., Shanghai, China). All reagents and solvents were commercially available with chemical or analytical purity.

2.2. Fungi

Gibberella saubinetii (*G. saubinetii*), *Alternaria solani* (*A. solani*), *Thanatephorus cucumeris* (*T. cucumeris*), *Verticillium dahlia* (*V. dahlia*), and *Gibberella zeae (Schwein.) Petch* (*G. zeae*) were purchased from Beijing Beina Chuanglian Biotechnology Institute, China. *Botryosphaeria dothidea* (*B. dothidea*) was provided by GuiYang University and identified by Sangon Biotech (Shanghai) Co., Ltd., China. All fungi were grown on PDA plates at 25 ± 1 °C in the dark and maintained at 4 °C.

2.3. Mycelia and cultivating conditions

Five fresh mycelial dishes (4 mm) of *T. cucumeris* were cut from the PDA medium and added to PDB medium. They were cultivated at 25 °C and 180 rpm, and the mycelia were further treated in different ways according to the experimental requirements as follows:

(a) The hyphae were mixed and cultivated with different concentrations of target compounds (50.0, 25.0, and 10.0 μg/

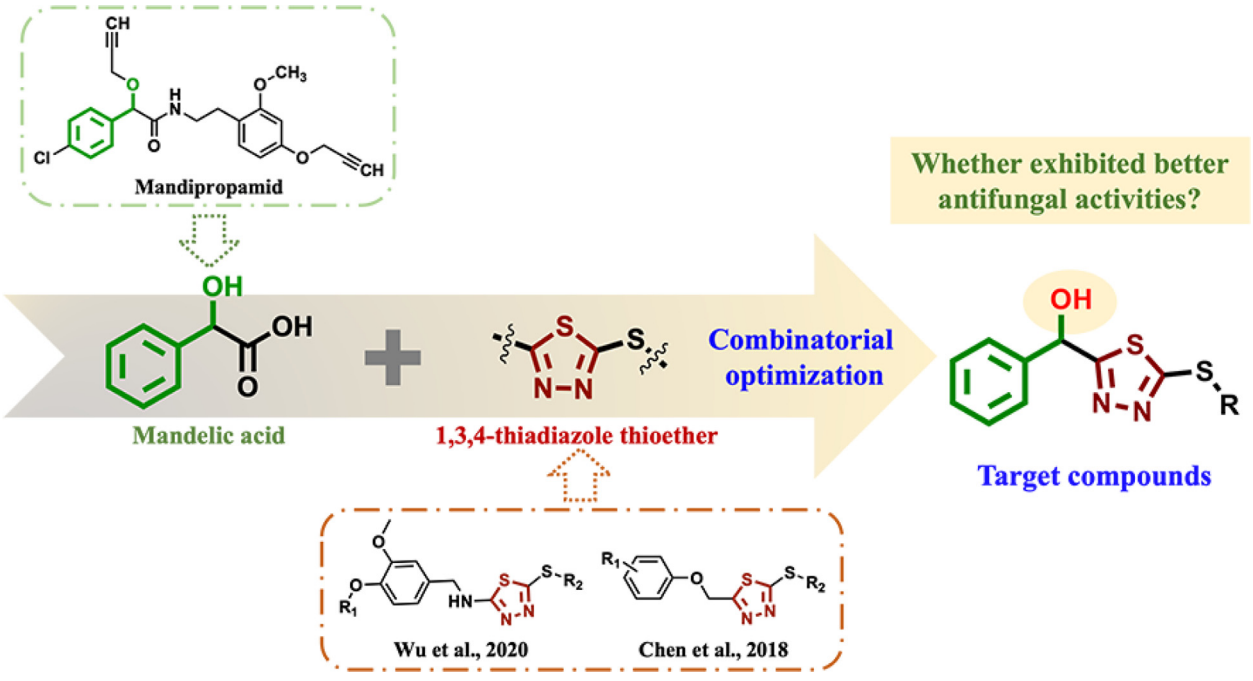

Fig. 1 The design strategy for the target compounds.

mL) for 96 h and filtered (Mo et al., 2021). The hyphae were washed 3 times with distilled water, dried at 65 °C for 12 h, and then used in mycelial weight experiments.

(b) After cultivation for 72 h and filtering, the hyphae were washed with distilled water 3 times, and then fresh hyphae (2.0 g) were put into PDB medium (50 mL) with different concentrations of target compounds (50.0, 25.0, and 10.0 μg/mL) and cultivated for 72 h under the same conditions and then filtered (Mo et al., 2021). The hyphae were washed 3 times with distilled water, dried at 65 °C for 12 h, and then used in mycelial loss ratio experiments.

(c) After cultivation for 48 h, different concentrations of $\mathbf{F_{10}}$ (50.0, 25.0, and 10.0 μg/mL) were added to the PDB medium, and the hyphae were incubated for 24 h under the same conditions and then filtered. Then, the hyphae were washed with PBS solution 3 times (Hou et al., 2018; Wang et al., 2019; Yang et al., 2019b) and used in the morphological study, cell membrane permeability study and MDA content determination experiments.

In all of the above experiments, the same volume of DMSO was used as the CK group, and the commercial agent triadimefon was used as a positive control.

2.4. Synthesis

2.4.1. General synthetic procedure for intermediate *B*

A mixture of *DL*-mandelic acid (**A**, 0.1 mol), 98% H_2SO_4 (1 mL), and CH_3OH (30 mL) was refluxed at 100 °C, monitored reacted by TLC for 3 h. Then, the solvent was evaporated under reduced pressure to get crude product, and separated by silica gel column chromatography (eluent: petroleum ether/ethyl acetate = 30/1) to obtain intermediate **B**.

2.4.2. General synthetic procedure for intermediate *C*

B (0.1 mol) was added in the solution of 80% $NH_2NH_2{\cdot}H_2O$ (0.4 mol), reacted for 2 h at r.t., then the mixture was filtered, and the crude product was purified by recrystallized with EtOH solution to obtain intermediate **C**.

2.4.3. General synthetic procedure for intermediate *d*

C (0.1 mol) were reacted with KOH (0.12 mol) and CS_2 (0.3 mol) in C_2H_5OH solution for 7 h at r.t., and the solvent was concentrated under reduced pressure. The crude product was slowly added into 98% H_2SO_4 (15 mL), reacted for 6 h at 0 °C. Then, the mixture was dropwise poured into ice water (90 mL), filtered, and purified by silica gel column chromatography (eluent: dichloromethane/ methanol = 100/1) to obtain intermediate **D**.

2.4.4. General synthetic procedure for intermediates *E*

A mixture of **D** (1.0 mmol), methanol (10 mL), and $NaBH_4$ (1.1 mmol) was stirred for 30 min at r.t. Then, the solvent was concentrated under reduced pressure, and the residue was purified by column chromatography on silica gel (eluent: PE/EA = 10/1 – 3/1) to obtain the Intermediates **E**.

2.4.5. General synthetic procedure for target compounds F_1–F_{30}

To a solution of **E** (1.0 mmol) in CH_3CN solution (8.0 mL), $(C_2H_5)_3N$ (0.5 mL) and different benzyl halides (1.2 mmol) were added and stirred for 24 h at r.t., then concentrated *in vacuo*. The residue was purified by silica gel column chromatography (eluent: PE/EA: 100/1 – 20/1) to obtain $\mathbf{F_n}$ (Sauer et al., 2017; Yang et al., 2021).

2.5. Crystallographic analysis of target compound F_{16}

A single crystal of target compound $\mathbf{F_{16}}$ suitable for X-ray diffraction analysis was obtained by slow evaporation of the solution (petroleum ether/ethyl acetate) at r.t. X-ray crystallographic data were collected by a Bruker Corporation diffractometer (Bruker Corporation, Germany). The crystal was kept at 293.15 K during data collection. Using Olex2, the structure was solved with the SHELXT structure solution program using Intrinsic Phasing and refined with the SHELXL refinement package using Least Squares minimization.

2.6. Effects on in vitro mycelial growth

In vitro antifungal activities of the key intermediates and target compounds against six plant pathogenic fungi (*G. saubinetii*, *A. solani*, *T. cucumeris*, *V. dahliae*, *G. zeae*, and *B. dothidea*) were evaluated using a mycelial growth inhibition method with some modifications (Li et al., 2019b). The initial screening concentration was 100 μg/mL, 1% DMSO in sterile distilled water was used as a CK group, and the commercial fungicide triadimefon served as a positive control. Mycelia were incubated at 25 °C in the dark, and the diameters of the hyphae in the treatment groups were measured by the cross-crossing method when they reached approximately 6.0 cm in the CK groups.

The EC_{50} values of the target compounds that exhibited > 50% inhibitory effects at 100 μg/mL were further determined using the method described above. A gradient of concentrations of the test compounds of 200, 100, 50, 25, 12.5, 6.25, and 3.125 μg/mL were prepared.

2.7. Effect of treatment with F_{10} on the hyphae weight and loss ratio of T. Cucumeris

The weight of the hyphae cultivated with method (a) described above was calculated after the hyphae were dried. The loss ratio of the hyphae cultivated with method (b) described above was calculated with the formula: I (%) = [(W − R)/(W)] × 100, where W represents the dry weight of the initial hyphae and R represents the residual weight of the CK group or the treated group (Mo et al., 2021).

2.8. Effect on sclerotia formation and germination

The hyphae were cultivated on PDA medium containing various concentrations (25.0 and 50.0 μg/mL) of $\mathbf{F_{10}}$ in the dark at 25 °C for 14 continuous days and photographed and recorded by SM.

The sclerotia germination inhibitory experiment was performed using the method described previously with some modifications. First, *T. cucumeris* were incubated in the dark for 14 d to obtain sclerotia; then, PDA plates containing different concentrations of $\mathbf{F_{10}}$ (25.0 and 50.0 μg/mL) were prepared; finally, 15 sclerotia were picked and placed on each PDA plate. DMSO and triadimefon were used as the CK and the positive control, respectively. All treatment groups were cultivated in

the dark at 25 °C for 72 h and then observed, photographed and recorded by SM. The inhibitory effect of **F_{10}** on sclerotia germination was calculated by the formula: I (%) = [(G − F)/(G − d)] × 100, where G represents the diameter of sclerotia germination of the CK group, F represents the diameter of sclerotia germination after treatment with **F_{10}**, and d represents the average diameter of sclerotia (Hou et al., 2018; Zhang et al., 2018).

2.9. In vivo activity against rice sheath blight

The rice plants were cultivated and used to evaluate the protective and curative activities against rice sheath blight infected with *T. cucumeris*. For the protective activity, the rice plants were treated with target compound **F_{10}** by spraying with 200 μg/mL and then inoculated with one *T. cucumeris* sclerotia (2 mm) 24 h later on a leaf sheaf of each plant. However, for the curative activity, the plants were first inoculated with *T. cucumeris* sclerotia for 24 h and then sprayed with **F_{10}** (200 μg/mL). All of the treatments were replicated for the same batch plants and maintained at 25 ± 1 °C and 90% RH with a 12 h light/12 h dark photoperiod, the same volume of DMSO was used as the CK group, with triadimefon as a positive control. The control efficacies were calculated as follows after 7 d of inoculation: control efficacy (%) = $(D_0\text{-}D_1)/D_0 \times 100\%$, where D_0 and D_1 are the diameters of the CK and the treatment group, respectively (Zhang et al., 2018).

2.10. Morphological study of mycelia from T. cucumeris by SEM and FM

After fixation with 2.5% glutaraldehyde at 4 °C for 24 h, the hyphae were washed with PBS 3 times before being dehydrated with a series of ethanol solutions (30%, 50%, 70%, 90% anhydrous ethanol and 100% tertiary butanol). Then, the hyphae were observed by SEM after freeze drying and gold-spraying (Yang et al., 2019b).

The PBS solution with hyphae in a 2 mL centrifuge tube was removed by centrifuging at 4 °C and 6000 rpm for 5 min. A PI solution of 1/10 PBS volume (10.0 μg/mL) was added to the centrifuge tube for staining after the supernatant was removed. The centrifuge tube was wrapped in tin foil and incubated in a thermostatic mixer at 37 °C and 1000 rpm in the dark for 15 min. After coloring, the hyphae were washed with PBS 3 times, observed and photographed by FM (Yang et al., 2019b).

2.11. Study on cell membrane permeability

The relative permeability of the cell membrane of *T. cucumeris* was evaluated according to a previous method with some modifications. The hyphae were washed with distilled water three times and filtered. Hyphae (2.0 g) were added to a beaker containing 50 mL distilled water and shaken well, and the electrical conductivity of mycelia was measured at 0, 1, 2, 4, 6, 8, 10, and 12 h (electrical conductivity at each time point). After 12 h, the beaker was placed in a boiling water bath for 5 min, and the absolute electrical conductivity was measured and calculated with the formula: relative conductivity (%) = electrical conductivity at each time/absolute electrical conductivity × 100% (Wang et al., 2017; Wang et al., 2019; Elsherbiny et al., 2021).

2.12. MDA content determination of mycelia

The hyphae were washed with distilled water 3 times and filtered under vacuum for 10 min. Then, 0.1 g hyphae were added to 1.0 mL MDA extract solution (produced by Beijing Solaibao Technology Co., Ltd., Beijing, China), homogenized in a tissue morcellator, and centrifuged at 8000 g and 4 °C for 15 min. The supernatant was removed, and MDA content was determined using an MDA detection kit (Beijing Solaibao Technology Co., Ltd., China) (Yang et al., 2020; Mo et al., 2021).

2.13. Data analysis

The EC_{50} values were calculated with Origin 2021 software by regression equation and R^2. All treatments were performed with three replicates by conventional methods, and data in the same groups were evaluated by the deviation value test. The results are presented as the means ± SDs. To determine the effects of the treatments, all the data in the study were analyzed using SPSS software version 18.0 (SPSS Inc., Chicago, IL, USA) for statistical variances (ANOVA) between repeated experiments to determine whether there were significant differences among the biological characteristics. A Duncan's multiple range test was used for mean separations when the treatment effects were statistically significant ($P < 0.05$).

3. Results and discussion

3.1. Synthesis

The synthetic route of the target compounds is shown in Fig. 2. Intermediate **B** was obtained by esterification of the raw material *DL*-mandelic acid (**A**) and then hydrazinolysis was performed to obtain intermediate **C**. CS_2 and KOH were added to form the transition state hydrazine salt and then cyclized in the presence of 98% H_2SO_4 at 0 °C to obtain intermediate **D**, reducing **D** obtained intermediate **E**, which was electrophilically substituted to form **E** obtained the target compounds **F_n**. The intermediates and target compounds were characterized by ^1H, ^{13}C, ^{19}F NMR and HRMS. The physical data and copies are provided in the Supporting Information.

3.2. Crystal structure of target compound F_{16}

As shown in Fig. 3, the crystal structure of **F_{16}** was confirmed via X-ray diffraction analysis. Crystallographic data of compound **F_{16}**: $C_{17}H_{16}N_2O_2S_2$ (M = 344.44 g/mol): monoclinic, space group $P2_1/c$ (no. 14), a = 9.5745(12) Å, b = 7.6138 (10) Å, c = 23.623(3) Å, β = 92.271(5)°, V = 1720.7(4) Å^3, Z = 4, T = 293.15 K, μ(CuKα) = 2.890 mm^{-1}, and *Dcalc* = 1.330 g/cm^3; 11,899 reflections were measured ($7.49° \leq 2\Theta \leq 144.152°$), and 3279 reflections were unique (R_{int} = 0.1979, R_{sigma} = 0.1657) and were used in all calculations. The final R_1 was 0.1532 ($I > 2\sigma(I)$), and wR_2 was 0.5971 (all data). The crystallographic data of target compound **F_{16}** were deposited in the Cambridge Crystallographic Data Cen-

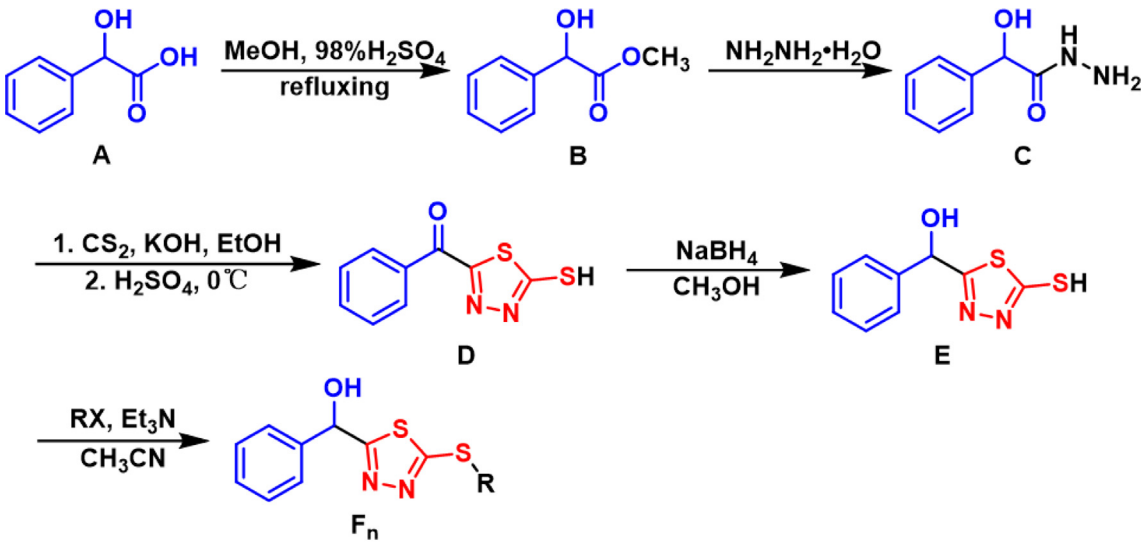

F_1: R=CH_3 **F_2**: R=CH_2CH_3 **F_3**: R=$CH_2CH_2CH_3$
F_4: R=$(CH_2)_3CH_3$ **F_5**: R=$(CH_2)_4CH_3$ **F_6**: R=$(CH_2)_{10}CH_3$
F_7: $CH_2CH(CH_3)_2$ **F_8**: R=$(CH_2)_2CH(CH_3)_2$ **F_9**: R=benzyl
F_{10}: R=2-methylbenzyl **F_{11}**: R=3-methylbenzyl **F_{12}**: R=4-methylbenzyl
F_{13}: R=2-trifluoromethyl benzyl **F_{14}**: R=3-trifluoromethyl benzyl **F_{15}**: R=4-trifluoromethyl benzyl
F_{16}: R=2-methoxybenzyl **F_{17}**: R=3-methoxybenzyl **F_{18}**: R=4-methoxybenzyl
F_{19}: R=2-trifluoro-methoxybenzyl **F_{20}**: R=3-trifluoro-methoxybenzyl **F_{21}**: R=4-trifluoro-methoxybenzyl
F_{22}: R=2-fluorine benzyl **F_{23}**: R=3-fluorine benzyl **F_{24}**: R=4-fluorine benzyl
F_{25}: R=2-chloride benzyl **F_{26}**: R=3-chloride benzyl **F_{27}**: R=4-chloride benzyl
F_{28}: R=2-bromine benzyl **F_{29}**: R=3-bromine benzyl **F_{30}**: R=4-bromine benzyl

Fig. 2 Synthetic route of the target compounds **F_1**–**F_{30}**.

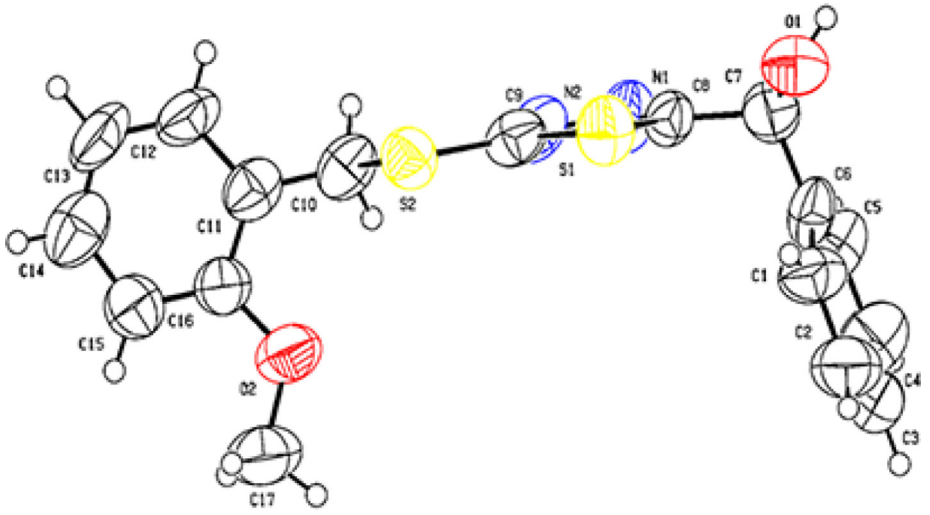

Fig. 3 Single crystal structure of **F_{16}**.

tre (CCDC) under deposition number 2159799. The detailed crystallographic data are provided in Table S1 in the Supporting Information.

3.3. Effects of mycelial growth treated with target compounds

Preliminary *in vitro* antifungal activity results of target compounds against six pathogenic fungi are provided in Table S2 in the Supporting Information, and revealed that most target compounds exhibited better antifungal bioactivities against *G. saubinetii* and *T. cucumeris*. As shown in Table 1, the EC_{50} value of **F_{15}** against *G. saubinetii* was 11.4 μg/mL, similar to that of triadimefon (14.8 μg/mL); the EC_{50} values of **F_4**, **F_9**, **F_{10}**, and **F_{11}** against *T. cucumeris* were 15.3, 11.8, 9.7, and 18.7 μg/mL, respectively, similar to that of triadimefon (11.0 μg/mL). Structure-activity relationship (SAR) analysis

Table 1 EC_{50} values of partial target compounds against five pathogenic fungi.[a]

No.	EC_{50} value ± SDs (μg/mL) [a]				
	G. saubinetii	*A. solani*	*V. dahlia*	*G. zeae*	*T. cucumeris*
F_3	102.8 ± 3.5	91.9 ± 2.0	–	–	31.3 ± 0.6
F_4	84.2 ± 0.6	119.0 ± 4.7	–	–	15.3 ± 0.8
F_9	86.8 ± 0.8	62.5 ± 1.6	–	87.3 ± 1.7	11.8 ± 0.1
F_{10}	23.3 ± 0.1	50.0 ± 1.4	88.4 ± 0.8	63.0 ± 1.8	9.7 ± 0.1
F_{11}	28.0 ± 1.1	45.9 ± 1.9	89.2 ± 0.7	54.9 ± 1.3	18.7 ± 0.8
F_{13}	43.3 ± 0.5	42.3 ± 3.1	58.7 ± 1.3	104.0 ± 1.2	35.4 ± 1.1
F_{14}	52.2 ± 2.4	37.1 ± 0.3	73.4 ± 0.8	112.7 ± 4.1	27.7 ± 0.4
F_{15}	11.4 ± 0.2	36.6 ± 1.5	69.6 ± 2.4	167.5 ± 10.9	46.1 ± 0.7
F_{16}	92.7 ± 1.0	37.0 ± 1.8	–	–	–
F_{17}	90.1 ± 1.4	63.8 ± 0.2	–	108.1 ± 1.4	25.7 ± 1.7
F_{19}	47.6 ± 2.3	56.4 ± 1.1	66.2 ± 1.1	55.3 ± 2.0	51.2 ± 1.2
F_{20}	37.6 ± 1.6	42.1 ± 0.9	72.1 ± 0.8	49.1 ± 0.5	20.0 ± 0.4
F_{21}	23.6 ± 1.1	41.2 ± 1.8	72.9 ± 1.5	33.7 ± 1.3	24.3 ± 0.3
F_{22}	69.2 ± 1.0	70.5 ± 0.5	–	–	–
F_{23}	37.1 ± 1.3	49.6 ± 1.3	110.6 ± 4.6	81.4 ± 2.6	34.9 ± 1.0
F_{24}	47.7 ± 0.6	76.4 ± 1.4	102.9 ± 1.1	119.9 ± 2.5	32.7 ± 1.1
F_{25}	43.9 ± 0.3	35.8 ± 1.6	–	93.8 ± 2.4	60.6 ± 3.4
F_{26}	31.4 ± 0.8	47.1 ± 1.3	95.8 ± 0.8	86.3 ± 3.9	32.3 ± 1.0
F_{28}	49.2 ± 2.6	53.2 ± 2.1	175.8 ± 4.7	92.3 ± 4.0	116.4 ± 3.8
F_{29}	91.0 ± 3.8	48.2 ± 1.8	–	122.9 ± 7.0	53.9 ± 0.1
triadimefon	14.8 ± 0.5	45.3 ± 0.6	2.9 ± 0.2	16.9 ± 0.1	11.0 ± 0.7

[a] Values are the mean ± SDs of three replicates; "–" not tested.

indicated that compounds exhibited better antifungal activities when substituted group were introduced to 1,3,4-thiadizazole-2-thiol part. Compared the antifungal activities against six pathogenic fungi (*A. solani*, *G. saubinetii*, *V. dahlia*, *G. zeae*, *T. cucumeris* and *B. dothidea*) between **E** and **F_n** in Table S2, we found that most compounds with substituted group exhibited better antifungal activities than that with thioether group, especially when benzyl and substituted-benzyls were introduced to 1,3,4-thiadizazole-2-thiol part. In addition, as shown in Table S2 to S4, among 'R' groups, most compounds with benzyl and substituted-benzyls group exhibited better antifungal activities than that with alkyl group, especially when benzyl, 2-methylbenzyl, and 4-trifluoromethyl benzyl were introduced to 1,3,4-thiadizazole-2-thiol part. Moreover, the antifungal activity of the most title compounds with the *meta*-substituted were generally better than that of the compounds with *para*-substituent, such as **F_{11}**, **F_{23}**, and **F_{26}** (the EC_{50} values were 28.9, 37.1, and 31.4 μg/mL, respectively), which were better than that of **F_{12}**, **F_{24}**, and **F_{27}** against *G. saubinetii*; **F_{11}**, **F_{14}**, **F_{17}**, **F_{20}**, and **F_{26}** (the EC_{50} values were 18.7, 27.7, 25.7, 20.0, and 32.3 μg/mL, respectively) were better than that of **F_{12}**, **F_{15}**, **F_{18}**, **F_{21}**, and **F_{27}** against *T. cucumeris*. When **R** = methylbenzyl, the activity of title compounds with the *ortho*- and *meta*-substituted were mostly better than that of the compound with *para*-substituent, such as the EC_{50} values of **F_{10}** (9.7, 50.0, and 23.3 μg/mL), and **F_{11}** (18.7, 45.9, and 28.9 μg/mL) against *T. cucumeris*, *A. solani*, and *G. saubineti* both better than the *para*-substituent **F_{12}**. When **R** = tri fluoro-methoxybenzyl, the activity of title compound with the *para*-substituent was mostly better than that of the compound with *ortho*-substituted, such as **F_{21}** (24.3, 33.7, 41.2, and 23.6 μg/mL) was better than that of **F_{19}** (51.2, 55.3, 56.4, and 47.6 μg/mL) against *T. cucumeris*, *A. solani*, *G. zeae*, and *G. saubinetii*. The regression equations and R^2 are provided in Tables S3 and S4 in the Supporting Information.

As shown in Fig. 4A, compared with the dry weight of the hyphae in the CK group (310.7 mg), the dry weights of the hyphae of *T. cucumeris* treated with different concentrations of **F_{10}** (50.0, 25.0, and 10.0 μg/mL) were 5.7, 13.3, and 56.7 mg, respectively, which were less than those treated with triadimefon (47.7, 82.7, and 100.7 mg, respectively). The weight of hyphae was significantly decreased after treatment with different concentrations of **F_{10}** (50.0, 25.0, and 10.0 μg/mL), and the loss rates were 82.8%, 79.7% and 72.9%, respectively, which were all higher than those of triadimefon (74.1%, 68.1% and 60.5%, respectively) (Fig. 4B).

The dry weight of the hyphae of *T. cucumeris* gradually decreased with increasing **F_{10}** concentration, which was consistent with the result shown in Fig. 4C, revealing that the target compound **F_{10}** can effectively inhibit the growth of *T. cucumeris* hyphae. The loss rates of *T. cucumeris* reflected the weight loss of hyphae, and we speculated that target compound **F_{10}** may disrupt the structure of mycelium, leading to the leakage of substances in the hyphae, such as soluble sugars and proteins. Experiments for further verification were as follows.

*3.4. Sclerotia formation and germination of T. cucumeris treated with **F_{10}***

The sclerotia of *T. cucumeris* are an important primary infection source that can cause the disease of rice sheath blight, and the formation of sclerotia can be divided into three stages: sclerotia initial (SIs), sclerotia developing (SDs), and sclerotia mature (SMs) (Georgiou et al., 2006; Dong et al., 2018). As shown in Fig. 5, a small amount of sclerotia was formed after treatment with **F_{10}** at a concentration of 25 μg/mL from 7 d to 14 d, but the sclerotia were hardly formed after treatment with **F_{10}** at 50 μg/mL. In contrast, sclerotia can be formed under tri-

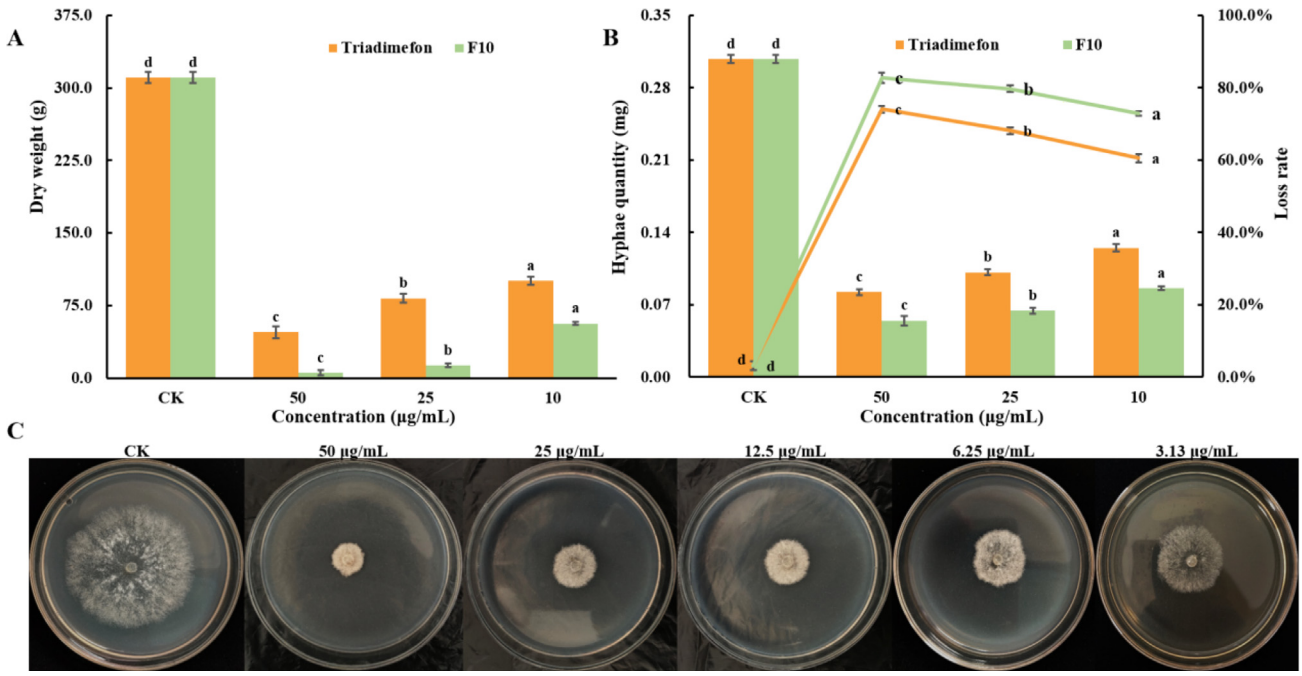

Fig. 4 **A:** The dry weight of hyphae treated with $\mathbf{F_{10}}$ and triadimefon; **B:** The loss rate of hyphae treated with $\mathbf{F_{10}}$ and triadimefon; **C:** Effect of treatment with $\mathbf{F_{10}}$ at different concentrations on the mycelial growth process. Error bars denote the standard error of the mean for three independent experiments. Different lowercase letters denote statistically significant differences at $P < 0.05$.

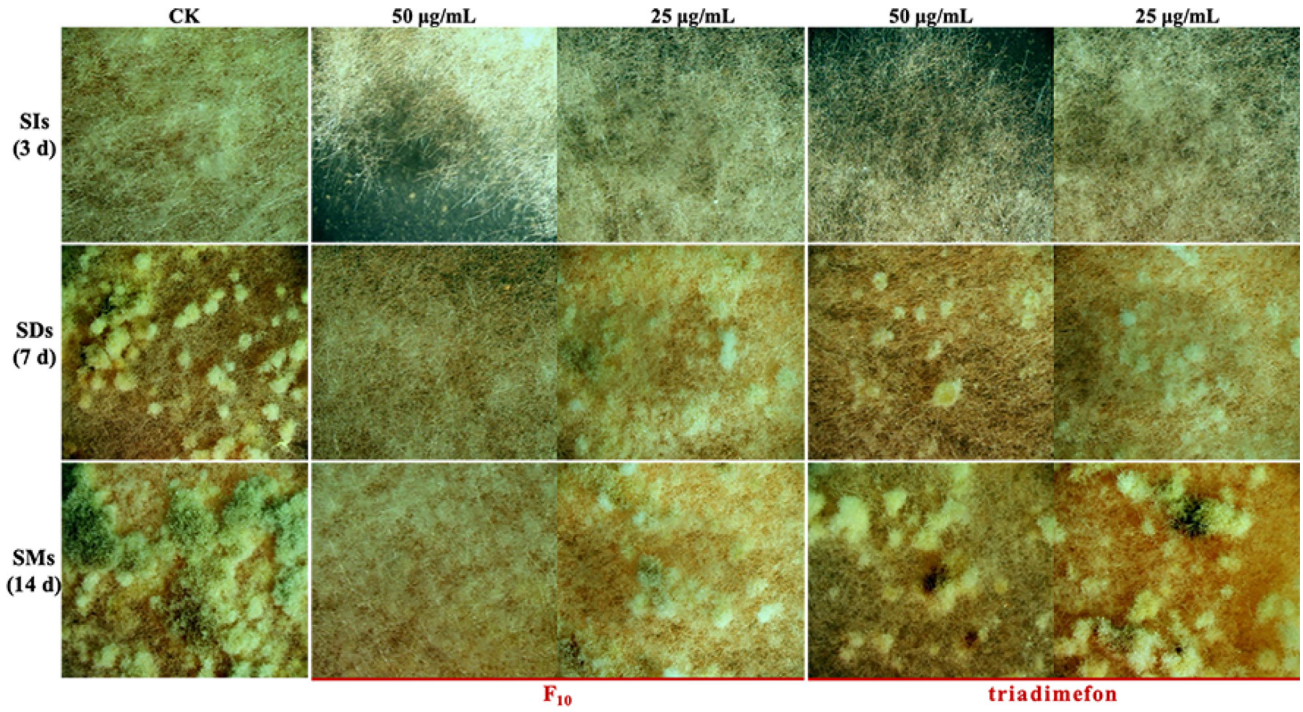

Fig. 5 Sclerotia formation of *T. cucumeris* treated with $\mathbf{F_{10}}$ and triadimefon.

adimefon treatment at concentrations of both 25 μg/mL and 50 μg/mL.

As shown in Fig. 6, the sclerotia germination rates all reached 100% after treatment with $\mathbf{F_{10}}$ and triadimefon at concentrations of 50 and 25 μg/mL. However, treatment with 50 and 25 μg/mL $\mathbf{F_{10}}$ slowed the speed of sclerotia germination, and the rates of slowdown were 38.5% and 24.2%, respectively, which were greater than those of triadimefon (28.8% and 22.5%, respectively).

After the target compound $\mathbf{F_{10}}$ treated the *T. cucumeris*, the number of formed sclerotia decreased or hardly formed. Compound $\mathbf{F_{10}}$ displayed excellent inhibitory activity. These results

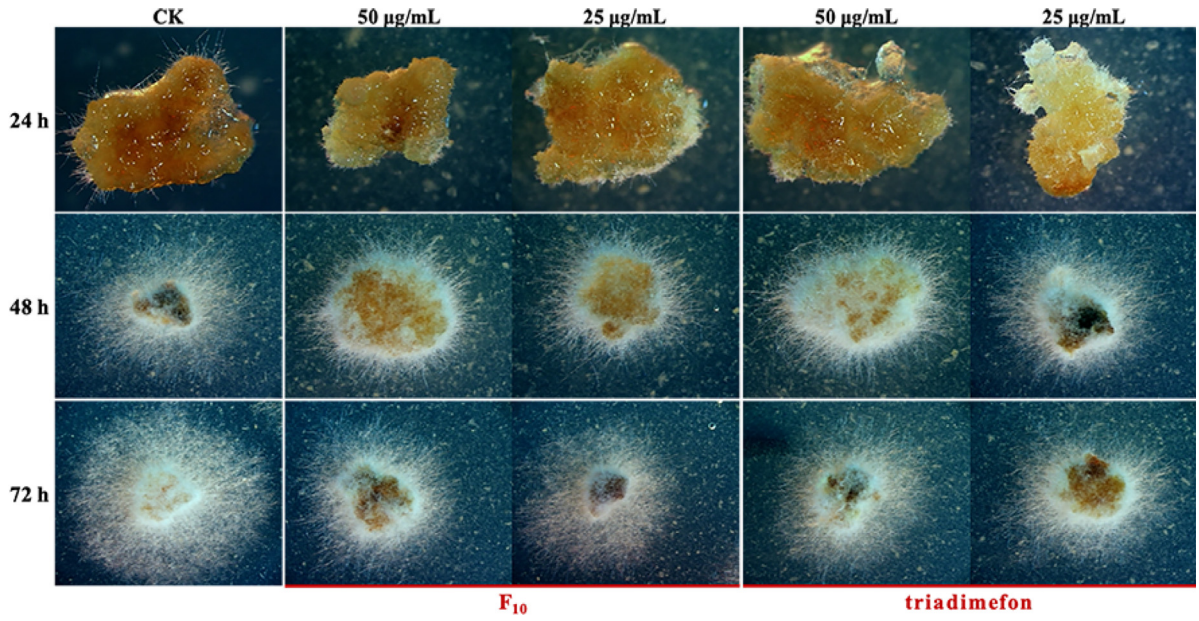

Fig. 6 Sclerotia germination of *T. cucumeris* treated with $\mathbf{F_{10}}$ and triadimefon.

revealed that compound $\mathbf{F_{10}}$ can effectively inhibit the sclerotia formation of *T. cucumeris* but had no obvious inhibitory activity against sclerotia germination. Combining the antifungal activity results, we found that $\mathbf{F_{10}}$ effectively inhibited the growth of hyphae and the formation of sclerotia, and hyphae were selected for further mechanism studies of $\mathbf{F_{10}}$ against *T. cucumeris*.

3.5. In vivo protective and curative activities treated with $\boldsymbol{F_{10}}$

As shown in Table 2 and Fig. 7, compound $\mathbf{F_{10}}$ exhibited significant *in vivo* curative (67.9%) and protective (61.1%) activities on rice plants leaf after inoculating with *T. cucumeris* sclerotia 7 d, which better than triadimefon (61.9% and 46.8%). And the results indicated that $\mathbf{F_{10}}$ exhibited excellent *in vivo* protective and curative activities against *T. cucumeris*, which could be used to control rice sheath blight.

3.6. Morphology study of the mycelia of T. cucumeris treated with $\boldsymbol{F_{10}}$

As shown in Fig. 8A and 8B, the mycelia of the CK group were regular in shape, uniform in thickness and complete in structure. However, the mycelia treated with $\mathbf{F_{10}}$ and triadimefon at different concentrations (50.0, 25.0, and 10.0 μg/mL) appeared uneven, wrinkled, irregularly shrunken, collapsed, and destroyed in a dose-dependent manner. Comparing the morphological changes of the hyphae under the treatment at the same concentration, we found that compound $\mathbf{F_{10}}$ had a more obvious effect than triadimefon.

PI is a fluorescent dye used to identify the membrane integrity of cells, and it can enter cells across damaged cellular membranes and emit red fluorescence (Yang et al., 2019b; Yang et al., 2020; Mo et al., 2021). Rather than passing through normal and intact cell membranes, the nucleus can be stained by a fluorescent dye that passes through damaged cell membranes (Mo et al., 2021; Xiao et al., 2021). As shown in Fig. 8C and 8D, no fluorescence was observed in the CK group, which indicated that the hyphae were intact and unharmed. The hyphae showed different degrees of fluorescence after treatment with $\mathbf{F_{10}}$ and triadimefon for 24 h at different concentrations. A small amount of red fluorescence was observed in the hyphae after the treatment at a low concentration (10 μg/mL), while greater fluorescence was observed at a high concentration (50 μg/mL), which indicated that as the concentration of the compounds increased, the hyphal breakage became more severe, consistent with the results observed by SEM.

Comprehensive analysis of the results of morphological studies demonstrated that $\mathbf{F_{10}}$ can obviously damage the mycelial shape of *T. cucumeris* and structural integrity. We speculated that $\mathbf{F_{10}}$ may affect the permeability of the cell membrane, and experiments for further verification were carried out.

Table 2 In vivo curative and protective activity of the $\mathbf{F_{10}}$ and triadimefon against *T. cucumeris* at 200 μg/mL.

	Curative activity		Protective activity	
Compound	Lesion length[a] (cm)	Control efficacy (%)	Lesion length[a] (cm)	Control efficacy (%)
$\mathbf{F_{10}}$	0.43 ± 0.10	67.9 ± 7.3	0.49 ± 0.13	61.1 ± 7.9
triadimefon	0.51 ± 0.14	61.9 ± 6.7	0.67 ± 0.13	46.8 ± 4.1
CK	1.34 ± 0.35	–	1.26 ± 0.20	–

[a] Values are the mean ± SDs of 3 replicates, each replicate was inoculated with 10 leaves.

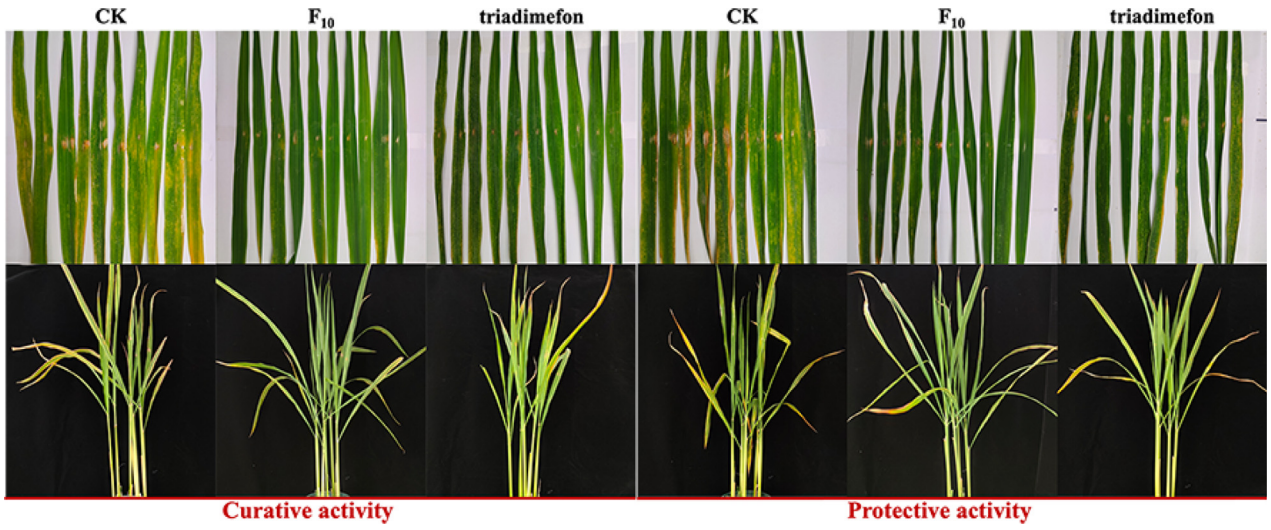

Fig. 7 In vivo curative and protective activities of $\mathbf{F_{10}}$ and triadimefon against *T. cucumeris* at 200 μg/mL.

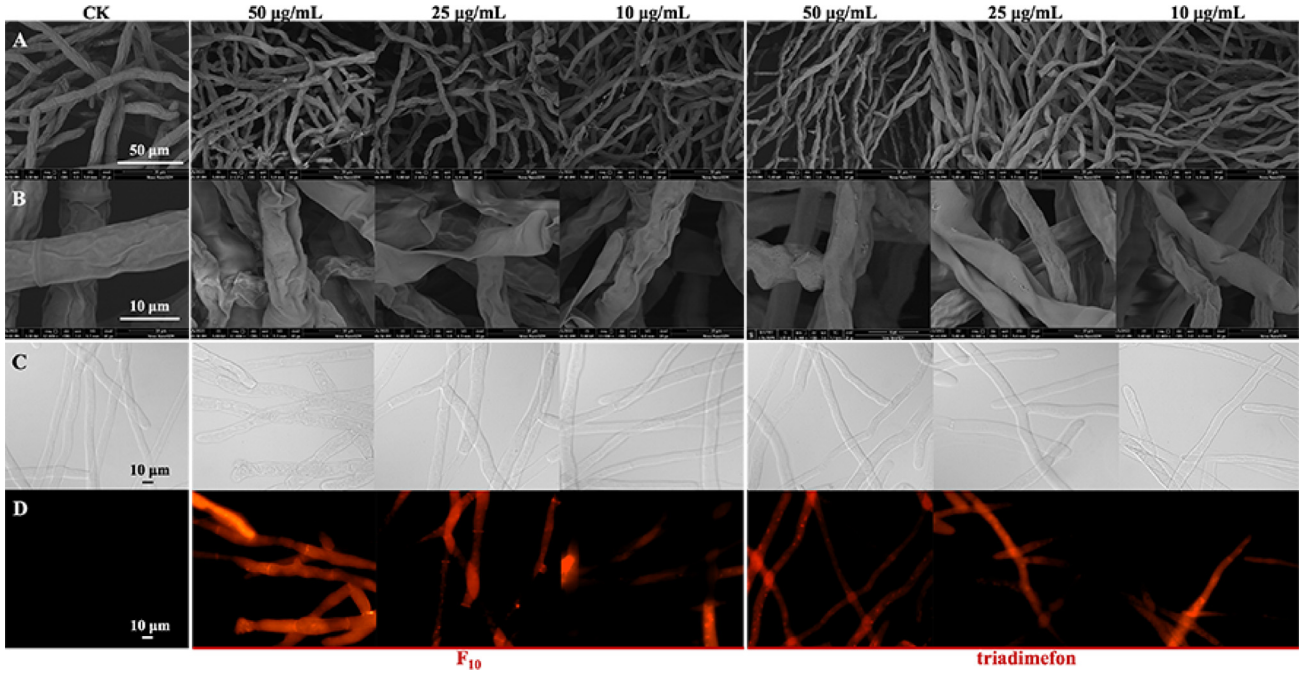

Fig. 8 Morphological observation of *T. cucumeris* treated with $\mathbf{F_{10}}$ and triadimefon. **A** and **B**: Observed by SEM; **C** and **D:** observed by FM; **C:** bright field; **D:** fluorescence field.

3.7. Cell membrane permeability of T. cucumeris treated with F_{10}

The conductivity changes of hyphae can reflect alterations in cell membrane permeability (Zhang et al., 2018). As shown in Fig. 9A, compared with the CK group, after treatment with $\mathbf{F_{10}}$ at different concentrations (50.0, 25.0, and 10.0 μg/mL), the relative electric conductivities of the hyphae were rapidly raised in a dose-dependent manner in the first 4 h, from 42.4% to 70.4%, from 41.6% to 65.9%, and from 38.7% to 58.9%, respectively. Then, the electrical conductivity increased slowly in each group from 4 h to 8 h, and the increases were 3.1, 6.0, and 11.5%, respectively. The increase tended to be mild from 8 to 12 h, at < 2.0%. The relative electrical conductivity data indicated that $\mathbf{F_{10}}$ may cause the leakage of substances (soluble sugars and proteins) in the hyphae and increase the ionic concentration. The results revealed that after $\mathbf{F_{10}}$ treatment, cell membrane permeability was obviously affected (Xin et al., 2020; Elsherbiny et al., 2021; Yang et al., 2021).

3.8. MDA content for mycelia of T. cucumeris treated with F_{10}

The MDA assay is an evaluation of membrane structure and one of the important indicators of integrity. The higher the

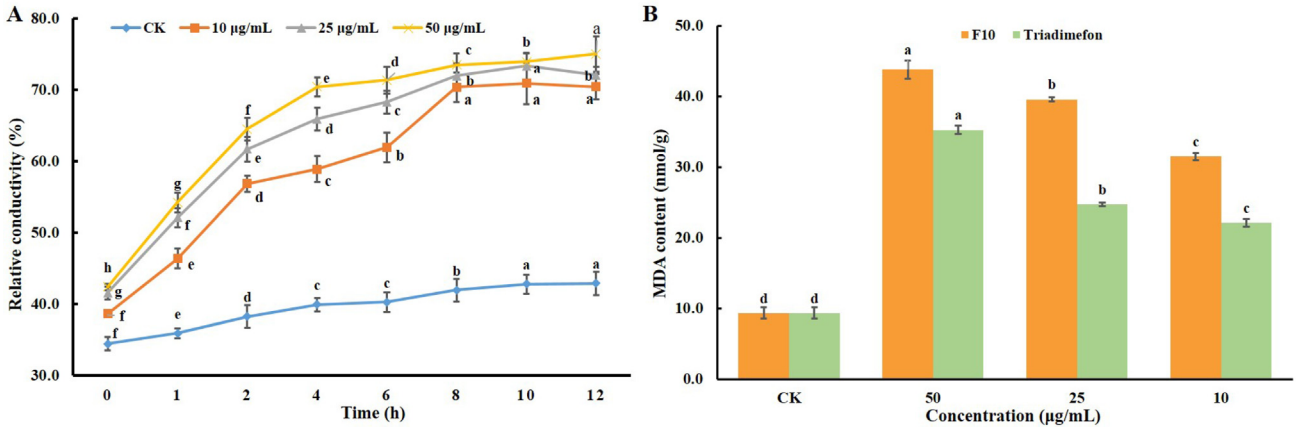

Fig. 9 **A:** Cell membrane permeability of the hyphae of *T. cucumeris* treated with $\mathbf{F_{10}}$ at different concentrations and times; **B:** MDA content of hyphae treated with $\mathbf{F_{10}}$ and triadimefon at different concentrations (50.0, 25.0, and 10.0 μg/mL). Error bars denote the standard error of the mean for three independent experiments. Different lowercase letters denote statistically significant differences at $P < 0.05$.

MDA content is, the more serious the damage is to the cell membrane (Yang et al., 2019b; Yang et al., 2021). As shown in Fig. 9B, the MDA content of hyphae after $\mathbf{F_{10}}$ treatment for 24 h was obviously higher than that of the CK group, and the MDA content was increased by 368.1%, 322.9% and 236.8% after treatment with different concentrations of $\mathbf{F_{10}}$ (50.0, 25.0, and 10.0 μg/mL, respectively), which were all greater increases than those with triadimefon treatment. Combining the results of morphology, cell membrane permeability and MDA content studies, we found that target compound $\mathbf{F_{10}}$ can obviously damage the cell membranes of mycelia from *T. cucumeris* at lower concentrations (10 μg/mL).

The sclerotia and mycelia are both important infection sources for plant diseases. In this work, target compound $\mathbf{F_{10}}$ with high antifungal activity against *T. cucumeris* was further studied, and the results revealed that $\mathbf{F_{10}}$ can inhibit the sclerotia formation of *T. cucumeris* and break the cell membranes of mycelia, which affects the growth of mycelia, and exhibited excellent *in vivo* protective and curative activities. All results of this study demonstrated that this series of compounds with high activity can be used to effectively control rice sheath blight which infected with *T. cucumeris*.

4. Conclusion

In summary, thirty novel mandelic acid derivatives containing 1,3,4-thiadiazole thioether were designed and synthesized. Bioassay evaluation revealed that most target compounds exhibited excellent antifungal activities against *T. cucumeris*; among them, the EC_{50} value of $\mathbf{F_{10}}$ was 9.7 μg/mL. Further studies found that $\mathbf{F_{10}}$ not only significantly inhibited the growth of *T. cucumeris* mycelia but also effectively inhibited the formation of sclerotia in *T. cucumeris*. Morphology studies of the mycelium showed that $\mathbf{F_{10}}$ can obviously affect the mycelium shape and structural integrity of *T. cucumeris*. Further mechanism studies demonstrated that this series of target compounds can damage the integrity of the cell membrane structure, resulting in increased permeability of the cell membrane, release of intracellular electrolytes and inhibition of fungal growth. In general, target compounds can significantly inhibit the growth of *T. cucumeris* hyphae and the formation of sclerotia *in vitro* and effectively control the diseases caused by *T. cucumeris in vivo*, which is helpful for managing the formation and diffusion of the infection sources and provides an effective method to control rice sheath blight disease.

Declaration of Competing Interest

The authors declare that they have no known competing financial interests or personal relationships that could have appeared to influence the work reported in this paper.

Acknowledgments

This work was supported by the National Natural Science Foundation of China (Nos. 32160655, 21662008), and Breeding Program of Guizhou University (No. 201931).

Appendix A. Supplementary data

Supplementary data to this article can be found online. They including ^{1}H NMR, ^{13}C NMR, ^{19}F NMR and HRMS spectra data and pictures for intermediates and target compounds; crystallographic data of target compound $\mathbf{F_{16}}$; *in vitro* antifungal activity results of target compounds: the regression equations and R^2 of the target compounds.

Supplementary data to this article can be found online at https://doi.org/10.1016/j.arabjc.2023.104884.

References

Ashkani, S., Rafii, M.Y., Shabanimofrad, M., et al, 2015. Molecular breeding strategy and challenges towards improvement of blast disease resistance in rice crop. Front. Plant Sci. 6. https://doi.org/10.3389/fpls.2015.00886.

Basu, A., Chowdhury, S., Ray, C.T., et al, 2016. Differential behaviour of sheath blight pathogen *Rhizoctonia solani* in tolerant and susceptible rice varieties before and during infection. Plant Pathol. 65, 1333–1346. https://doi.org/10.1111/ppa.12502.

Chen, Z., Li, D., Xu, N., et al, 2019c. Novel 1,3,4-selenadiazole-containing kidney-type glutaminase inhibitors showed improved cellular uptake and antitumor activity. J. Med. Chem. 62 (2), 589–603. https://doi.org/10.1021/acs.jmedchem.8b01198.

Chen, J., Yi, C., Wang, S., et al, 2019a. Novel amide derivatives containing 1,3,4-thiadiazole moiety: Design, synthesis, nematocidal and antibacterial activities. Bioorg. Med. Chem. Lett. 29 (10), 1203–1210. https://doi.org/10.1016/j.bmcl.2019.03.017.

Chen, L., Zhao, B., Fan, Z., et al, 2019b. Discovery of novel isothiazole, 1,2,3-thiadiazole, and thiazole-based cinnamamides as fungicidal candidates. J. Agric. Food Chem. 67 (45), 12357–12365. https://doi.org/10.1021/acs.jafc.9b03891.

Dong, J., Gao, W., Li, K., et al, 2022. Design, synthesis, and biological evaluation of novel psoralen-based 1,3,4-oxadiazoles as potent fungicide candidates targeting Pyruvate kinase. J. Agric. Food Chem. 70 (11), 3435–3446. https://doi.org/10.1021/acs.jafc.1c07911.

Dong, C., You, W., Liu, Y.R., et al, 2018. Anti-*Rhizoctonia solani* activity by polymeric quaternary ammonium salt and its mechanism of action. React. Funct. Polym. 125, 1–10. https://doi.org/10.1016/j.reactfunctpolym.2018.01.020.

El, S.N., Gould, I.M., 2016. Role of old antimicrobial agents in the management of urinary tract infection. Expert Rev. Clin. Pharmacol. 9 (8), 1047–1056. https://doi.org/10.1080/17512433.2016.1189325.

Elsherbiny, E.A., Dawood, D.H., Safwat, N.A., 2021. Antifungal action and induction of resistance by β-aminobutyric acid against *Penicillium digitatum* to control green mold in orange fruit. Pestic. Biochem. Physiol. 171,. https://doi.org/10.1016/j.pestbp.2020.104721 104721.

Feng, S.J., Shu, C.W., Wang, C.J.Z., et al, 2017. Survival of *Rhizoctonia solani* AG1 IA, the causal agent of rice sheath blight, under different environmental conditions. J. Phytopathol. 165, 44–52. https://doi.org/10.1111/jph.12535.

Fisher, M.C., Henk, D.A., Briggs, C.J., et al, 2012. Emerging fungal threats to animal, plant and ecosystem health. Nature. 484 (7393), 186–194. https://doi.org/10.1038/nature10947.

Gan, X., Hu, D., Chen, Z., et al, 2017. Synthesis and antiviral evaluation of novel 1,3,4-oxadiazole/thiadiazole-chalcone conjugates. Bioorg. Med. Chem. Lett. 27 (18), 4298–4301. https://doi.org/10.1016/j.bmcl.2017.08.038.

Georgiou, C.D., Patsoukis, N., Papapostolou, I., et al, 2006. Sclerotial metamorphosis in filamentous fungi is induced by oxidative stress. Integr. Comp. Biol. 46 (6), 691–712. https://doi.org/10.1093/icb/icj034.

Ghorbanpour, M., Omidvari, M., Abbaszadeh-Dahaji, P., et al, 2018. Mechanisms underlying the protective effects of beneficial fungi against plant diseases. Biol. Control. 117, 147–157. https://doi.org/10.1016/j.biocontrol.2017.11.006.

Giray, B., Karadag, A.E., Ipek, O.S., et al, 2020. Design and synthesis of novel cylopentapyrazoles bearing 1,2,3-thiadiazole moiety as potent antifungal agents. Bioorg. Chem. 95,. https://doi.org/10.1016/j.bioorg.2019.103509 103509.

Hou, Y., Mao, X., Qu, X., et al, 2018. Molecular and biological characterization of *Sclerotinia sclerotiorum* resistant to the anilinopyrimidine fungicide cyprodinil. Pestic. Biochem. Physiol. 146, 80–89. https://doi.org/10.1016/j.pestbp.2018.03.001.

Ke, Y., Deng, H., Wang, S., 2017. Advances in understanding broad-spectrum resistance to pathogens in rice. The Plant J. 90 (4), 738–748. https://doi.org/10.1111/tpj.13438.

Li, Y., Aioub, A.A.A., Lv, B., et al, 2019b. Antifungal activity of pregnane glycosides isolated from *periploca sepium* root barks against various phytopathogenic fungi. Ind. Crop. Prod. 132, 150–155. https://doi.org/10.1016/j.indcrop.2019.02.009.

Li, A., Cheng, C., Qi, W., et al, 2021. Combing multiple site-directed mutagenesis of penicillin G acylase from *Achromobacter xylosoxidans* PX02 with improved catalytic properties for cefamandole synthesis. Int. J. Biol. Macromol. 175, 322–329. https://doi.org/10.1016/j.ijbiomac.2021.01.194.

Li, J., Wang, R., Sun, Y., et al, 2019a. Design, synthesis and antifungal activity evaluation of isocryptolepine derivatives. Bioorg. Chem. 92,. https://doi.org/10.1016/j.bioorg.2019.103266 103266.

Lu, L., Shu, C., Liu, C., et al, 2016. The impacts of natural antioxidants on sclerotial differentiation and development in *Rhizoctonia solani* AG-1 IA. Eur. J. Plant Pathol. 146 (4), 729–740. https://doi.org/10.1007/s10658-016-0953-3.

Ma, W., Zhao, L., Zhao, W., et al, 2019. (*E*)-2-Hexenal, as a potential natural antifungal compound, inhibits Aspergillus flavus spore germination by disrupting mitochondrial energy metabolism. J. Agric. Food Chem. 67 (4), 1138–1145. https://doi.org/10.1021/acs.jafc.8b06367.

Mao, S., Wu, C., Gao, Y., et al, 2021. Pine rosin as a valuable natural resource in the synthesis of fungicide candidates for controlling *Fusarium oxysporumn* cucumber. J. Agric. Food Chem. 69 (23), 6475–6484. https://doi.org/10.1021/acs.jafc.1c01887.

Mo, F., Hu, X., Ding, Y., et al, 2021. Naturally produced magnolol can significantly damage the plasma membrane of *Rhizoctonia solani*. Pestic. Biochem. Physiol. 178,. https://doi.org/10.1016/j.pestbp.2021.104942 104942.

Persaud, R., Khan, A., Isaac, W., et al, 2019. Plant extracts, bioagents and new generation fungicides in the control of rice sheath blight in Guyana. Crop. Prot. 119, 30–37. https://doi.org/10.1016/j.cropro.2019.01.008.

Roese, A.D., Vidal, G.S., Zeviani, W.M., et al, 2018. Agricultural diversification reduces the survival period of *Sclerotinia sclerotiorum* sclerotia. Eur. J. Plant Pathol. 151 (3), 713–722. https://doi.org/10.1007/s10658-017-1405-4.

Saeed, A., Shahzad, D., Faisal, M., et al, 2017. Developments in the synthesis of the antiplatelet and antithrombotic drug (*S*)-clopidogrel. Chirality. 29 (11), 684–707. https://doi.org/10.1002/chir.22742.

Sauer, A.C., Leal, J.G., Stefanello, S.T., et al, 2017. Synthesis and antioxidant properties of organosulfur and organoselenium compounds derived from 5-substituted-1,3,4-oxadiazole/thiadiazole-2-thiols. Tetrahedron Lett. 58 (1), 87–91. https://doi.org/10.1016/j.tetlet.2016.11.106.

Sun, S., Chen, L., Huo, J., et al, 2022. Discovery of novel pyrazole amides as potent fungicide candidates and evaluation of their mode of action. J. Agric. Food Chem. 70 (11), 3447–3457. https://doi.org/10.1021/acs.jafc.2c00092.

Suwannarach, N., Kumla, J., Bussaban, B., et al, 2012. Biocontrol of *Rhizoctonia solani* AG-2, the causal agent of damping-off by *Muscodor cinnamomi* CMU-Cib 461. World J. Microb. Biot. 28 (11), 3171–3177. https://doi.org/10.1007/s11274-012-1127-x.

Tiwari, I.M., Jesuraj, A., Kamboj, R., et al, 2017. Host Delivered RNAi, an efficient approach to increase rice resistance to sheath blight pathogen (*Rhizoctonia solani*). Sci. REP-UK 7, (1). https://doi.org/10.1038/s41598-017-07749-w.

Tudi, M., Daniel, Ruan, H., et al, 2021. Agriculture development, pesticide application and its impact on the environment. Int. J. Env. Res. Pub. He. 18 (3), 1112. https://doi.org/10.3390/ijerph18031112.

Wang, B., Liu, F., Li, Q., et al, 2019. Antifungal activity of zedoary turmeric oil against *Phytophthora capsici* through damaging cell membrane. Pestic. Biochem. Physiol. 159, 59–67. https://doi.org/10.1016/j.pestbp.2019.05.014.

Wang, Y., Sun, Y., Zhang, Y., et al, 2017. Sensitivity and biochemical characteristics of *Sclerotinia sclerotiorum* to propamidine. Pestic. Biochem. Physiol. 135, 82–88. https://doi.org/10.1016/j.pestbp.2016.05.006.

Xiao, L., Niu, H., Qu, T., et al, 2021. Streptomyces sp. FX13 inhibits fungicide-resistant *Botrytis cinerea in vitro* and *in vivo* by producing oligomycina. Pestic. Biochem. Physiol. 175,. https://doi.org/10.1016/j.pestbp.2021.104834 104834.

Xin, W., Mao, Y., Lu, F., et al, 2020. *In vitro* fungicidal activity and in planta control efficacy of coumoxystrobin against *Magnaporthe oryzae*. Pestic. Biochem. Physiol. 162, 78–85. https://doi.org/10.1016/j.pestbp.2019.09.004.

Yan, Y., Yang, C., Shang, X., et al, 2020. Bioassay-guided isolation of two antifungal compounds from magnolia officinalis, and the mechanism of action of honokiol. Pestic. Biochem. Physiol. 170, 104705. https://doi.org/10.1016/j.pestbp.2020.104705.

Yang, R., Han, M., Fan, J., et al, 2021. Development of novel (+)-nootkatone thioethers containing 1,3,4-oxadiazole/thiadiazole moieties as insecticide candidates against three species of insect pests. J. Agric. Food Chem. 69 (51), 15544–15553. https://doi.org/10.1021/acs.jafc.1c05853.

Yang, Q., Wang, J., Zhang, P., et al, 2020. *In vitro* and *in vivo* antifungal activity and preliminary mechanism of cembratrien-diols against *Botrytis cinerea*. Ind. Crop. Prod. 154,. https://doi.org/10.1016/j.indcrop.2020.112745 112745.

Yang, D., Zhao, B., Fan, Z., et al, 2019a. Synthesis and biological activity of novel succinate dehydrogenase inhibitor derivatives as potent fungicide candidates. J. Agric. Food Chem. 67 (47), 13185–13194. https://doi.org/10.1021/acs.jafc.9b05751.

Yang, G.Z., Zhu, J.K., Yin, X.D., et al, 2019b. Design, synthesis, and antifungal evaluation of novel quinoline derivatives inspired from natural quinine alkaloids. J. Agric. Food Chem. 67 (41), 11340–11353. https://doi.org/10.1021/acs.jafc.9b04224.

Yin, X.D., Ma, K.Y., Wang, Y.L., et al, 2020. Design, synthesis, and antifungal evaluation of 8-Hydroxyquinoline metal complexes against phytopathogenic fungi. J. Agric. Food Chem. 68 (40), 11096–11104. https://doi.org/10.1021/acs.jafc.0c01322.

Zhang, Z., Jiang, Z., Zhu, Q., et al, 2018. Discovery of β-Carboline oxadiazole derivatives as fungicidal agents against rice sheath blight. J. Agric. Food Chem. 66 (37), 9598–9607. https://doi.org/10.1021/acs.jafc.8b02124.